High latitude gas in the beta Pictoris system. A possible origin related to falling evaporating bodies

Hervé Beust, Pierre Valiron

A&A 466, 201–213 (2007)
DOI: 10.1051/0004-6361:20053425

Astronomy & Astrophysics

High latitude gas in the β Pictoris system

A possible origin related to falling evaporating bodies⋆

H. Beust and P. Valiron

Laboratoire d'Astrophysique de Grenoble, UMR 5571 CNRS, Université J. Fourier, BP 53, 38041 Grenoble Cedex 9, France
e-mail: Herve.Beust@obs.ujf-grenoble.fr

Received 13 May 2005 / Accepted 15 December 2006

ABSTRACT

Context. The puzzling detection of Ca II ions at fairly high latitude ($\gtrsim$30°) above the outer parts of the β Pictoris circumstellar disk was recently reported. Surprisingly, this detection does not extend to Na I atoms, in contradiction with our modelling of the emission lines in and out of the mid-plane of the disk.
Aims. We propose that the presence of these off-plane Ca II ions (and to a lesser extent Fe I atoms), and the non-detection of off-plane Na I atoms, could be the consequence of the evaporation process of Falling Evaporating Bodies (FEBs), i.e., star-grazing planetesimals that evaporate in the immediate vicinity of the star.
Methods. Our model is two-fold. Firstly, we show numerically and theoretically that in the star-grazing regime, the FEBs are subject to inclination oscillations up to 30–40°, and that most metallic species released during each FEB sublimation keep track of their initial orbital inclination while starting a free expansion away from the star, blown out by a strong radiation pressure. Secondly, the off-plane Ca II and Fe I species must be stopped prior to their detection at rest with respect to the star, about 100 AU away. We revisit the role of energetic collisional processes, and we investigate the possible influence of magnetic interactions.
Results. This dynamical process of inclination oscillations explains the presence of off-plane Ca II (and Fe I). It also accounts for the absence of Na I because once released by the FEBs, these atoms are quickly photoionized and no longer undergo any significant radiation pressure. Our numerical simulations demonstrate that the deceleration of metallic ions can be achieved very efficiently if the ions encounter a dilute neutral gaseous medium. The required H I column density is reduced to $\sim 10^{17}$ cm^{-2}, one order of magnitude *below* present detection limits. We also investigate the possibility that the ions are slowed down magnetically. While the sole action of a magnetic field of the order of 1 μG is not effective, the combined effect of magnetic and collisional deceleration processes lead to an additional lowering of the required H I column density by one order of magnitude.

Key words. stars: circumstellar matter – stars: individual: β Pic – celestial mechanics – methods: numerical – molecular processes – magnetic fields

1. Introduction

The dusty and gaseous disk surrounding the young main-sequence star β Pictoris has been the subject of intense investigation since its discovery (Smith & Terrile 1984). The main motivation for these studies is that this disk constitutes the most convincing example of a probable young extrasolar planetary system, possibly analogous to the early solar system. β Pic is a young star, but it is not a pre-main sequence star. Its age has been subject to controversy in past years, but successive determinations based on the kinematics of the socalled βPictoris moving group (Barrado y Navascués et al. 1999; Zuckerman et al. 2001; Ortega et al. 2004) lead to a most recent estimate of 11.2 Myr (Ortega et al. 2004). This shows that its disk should be called a *young planetary* rather than a *protoplanetary* disk, meaning that planet formation already should have had enough time to occur. Indeed, although no direct planet detection has been made so far, several indirect observational facts suggest that planets are present in the disk. This mainly concerns asymmetries found in the disk images from both scattered stellar light by the dust (Kalas & Jewitt 1995; Heap et al. 2000) and thermal emission by the dust (Weinberger et al. 2003), that have been modelled as resulting from the gravitational perturbations by one Jupiter-sized planet (Mouillet et al. 1997; Heap et al. 2000; Augereau et al. 2001).

The gaseous counterpart of the dust disk was detected in absorption in the stellar spectrum (Hobbs et al. 1985), and has been regularly observed since that time. Observations of many metallic species such as Na I, Ca II, Fe II... have been reported (Vidal-Madjar et al. 1994), extending more recently to more fragile species like CO (Jolly et al. 1998; Lecavelier des Etangs et al. 2001).

The gas was first detected at rest with respect to the star, but Doppler-shifted, highly time-variable components are regularly observed in the spectral lines of many elements (Ferlet et al. 1987; Lagrange et al. 1996; Petterson & Tobin 1999). These transient spectral events have been successfully modelled as resulting from the sublimation of numerous star-grazing planetesimals (several hundred per year) in the immediate vicinity of the star (see Beust et al. 1998, 1996, and refs. therein). This scenario has been termed the *Falling Evaporating Bodies* scenario (FEBs).

From a dynamical point of view, the origin of these numerous star-grazers seem to be related to mean-motion resonances (mainly 4:1 and 3:1) with a Jovian planet orbiting the star

⋆ Appendices are only available in electronic form at
http://www.aanda.org

on a moderately eccentric orbit ($e' \simeq 0.07$–0.1) (Beust & Morbidelli 1996, 2000). In this context though, the suspected resonance reservoirs are expected to clear out very quickly. In Thébault & Beust (2001), it was shown that collisions among the population of the planetesimals constituting the disk could help replenish the resonances from adjacent regions and subsequently sustain the FEB activity. However, there are still unsolved questions concerning this scenario. The main one concerns the amount of material available (Thébault et al. 2003). There is a large discrepancy between the number of planetesimals deduced from the FEB model and that deduced from an extrapolation of the dust observed population up to kilometre-sized bodies. We nevertheless note in Thébault et al. (2003) that the mass determination of Thébault & Beust (2001) from the FEB scenario is very imprecise as it is indirect. Indeed if the collisions are supplemented by some more violent transport processes, then the planetesimals population required to sustain the FEB activity could be much lower.

An important outcome of this model is that it implies an important reservoir of planetesimals in the disk and the presence of at least one giant planet at ~10 AU from the star. This is another argument in favour of the presence of planets in the β Pic disk. Moreover, the presence of numerous planetesimals is also a requirement of the dust models. Due to an intense radiation pressure, many dust particles should be quickly removed from the system. The particles observed consist of second generation material continuously replenished from inside the disk by planetesimals, either by slow evaporation (Lecavelier et al. 1996) or by collisions (Artymowicz 1997). This justifies the name *second generation* or *debris* disks given to the β Pic disk and other similar disks, such as the HD 141569 disk (see Augereau & Papaloizou 2004, and refs. therein).

Radiation pressure affects not only dust particles, but also the metallic species seen in absorption with respect to the star. Many of them undergo a radiation force from the star that largely overcomes the stellar gravity (Lagrange et al. 1998). This is for instance the case of Ca II for which the radiation pressure is 35 times larger than the stellar gravity. This seems in contradiction with the detection of circumstellar gas at rest with respect to the star. Lagrange et al. (1998) suggested that this stable gas was produced from inside by the FEBs themselves, that it is then blown away by the radiation pressure, and afterwards slowed down by a dense enough H I ring where it accumulates. The exact shape of this ring is of little importance, the main parameter being the integrated H I column density, of the order of 10^{18} cm^{-2}. Detailed modelling shows that all stable circumstellar lines can be reproduced this way.

In a recent paper, Brandeker et al. (2004, hereafter B04) report the detection with VLT/UVES of *emission* lines of metals (Fe I, Na I, Ca II) in the β Pic disk, i.e., away from the direction of the star. They report the detection of Na I and Fe I up to more than 300 AU from the star. Na I was resolved earlier by Olofsson et al. (2001), but the detection of B04 extends further out. H_2 was also claimed to be detected in emission by Thi et al. (2001), implying huge quantities (~50 $M_\oplus$) in the β Pic system, but this was questioned by Lecavelier des Etangs et al. (2001), who reported from FUSE/LYMAN observations an upper limit $N(H_2) \lesssim 10^{18}$ cm^{-2} for the H_2 column density towards β Pic.

A particularly puzzling outcome of the B04 observations is the detection of Ca II emission at fairly high latitude above the mid-plane of the disk. Ca II is detected at 77 AU height above and below the mid-plane at 116 AU from the star. This corresponds to an inclination of 33° above the mid-plane. At this distance, Ca II is detected in both branches of the disk and on both sides of the mid-plane, and the emission at 33° inclination largely overcomes that in the mid-plane. Surprisingly, the Fe I and Na I emission do not exhibit such a structuring. It is conversely concentrated in the mid-plane of the disk. However, the Fe I emission is broader than the Na I. At the height above the mid-plane corresponding to the peak emission in the Ca II lines, the Fe I is still detected. The gas shares the same radial velocity as the star within 1 or 2 km s^{-1} at most.

There is no straightforward explanation for the presence of species like Ca II *at such latitudes above the disk, nor for the absence of other species.* The purpose of this paper is to propose that this gas could constitute material released by the FEBs in the vicinity of the star, first blown away by radiation pressure, and then stopped far away from the star by friction with some gaseous medium, and/or by magnetic interaction. The Ca II and possibly the Fe I reach a significant inclination because the parent bodies (the FEBs) initially orbiting within the plane of the disk undergo inclination oscillations up so several tens of degrees when they reach the star-grazer state. Once released by the FEBs, the ions keep track of that inclination. In Sect. 2, we model the formation of the emission lines in and out of the mid-plane of the disk. We show that all the emissions are compatible with solar relative abundances between the elements under consideration, except that sodium should necessarily not be present (or strongly depleted) in the high latitude gas. In Sect. 3, we expose the dynamical model for high latitude gas generation, and we detail the theoretical background for inclination oscillations in the FEB state. We show that due to a negligible radiation pressure on Na II, sodium should not be present in this gas, in agreement with the observations.

In Sect. 4, we investigate how the Ca II ions could be slowed down at the stellar distance they are observed. We show that this deceleration can be achieved by collision with a dilute neutral medium, and we discuss the role of elastic and inelastic collisional processes. We also discuss the effect of a non-radial magnetic field. While the magnetic field in itself is inefficient to decelerate the ions, we show that its presence increases the efficiency of the deceleration by a neutral medium by an order of magnitude or more.

2. Modelling the emission lines

Our first task is to model the emission lines of Ca II, Na I and Fe I observed in and out of the mid-plane of the disk, as observed by B04. We focus on the Ca II K and H lines, the Na I D_1 and D_2 lines, and the Fe I $\lambda = 3859$ Å line. The modelling is done using the radiative transfer code CLOUDY by Ferland et al. (1998).

We take the synthetic ATLAS9 (Kurucz 1991) stellar model for βPic with $T_{\rm eff} = 8100$ K, $\log g = 4.207$ and a total luminosity of 8.7 $L_\odot$. We put gas at 116 AU from the star and compute the line emission. The chemical composition of the gas is assumed to be solar. The gas is modelled as a 10 AU wide layer with solar composition and a given hydrogen density.

Without any additional energy source other than the stellar radiation flux, the emission in all lines as computed by CLOUDY appears negligible, because the gas remains very cold (a few Kelvins). Thus, in order to generate detectable lines, the gas must be heated by some energy source. There can be some turbulence, but in the framework of our model, the strong deceleration of the weak flux of incoming metallic ions might constitute a sufficient heating source. In the following we thus assume the emission lines to be excited thermally. The incoming ions, once blown away by the radiation pressure, reach a velocity of ~10^3 km s^{-1} at 100 AU. The various surveys of the FEB

Table 1. Measured circumstellar ratios, and simulated emission intensities for the transitions under consideration. The circumstellar factors are taken from calibrated ESO/HARPS spectra of β Pic (Galland F., Priv. Comm.). The emission intensities (given in arbitrary units) out of the mid-plane are derived from the CLOUDY run and those in the mid-plane are estimated by multiplying the former ones by the circumstellar factors.

Transition	Circumstellar factor	Emission intensity above the mid-plane	Emission intensity in the mid-plane
Na I D_1	0.91	12.5	11.4
Na I D_2	0.90	24.8	22.3
Ca II K	0.033	15.8	0.521
Ca II H	0.0057	15.6	0.0889
Fe I 3859 Å	0.86	23.9	20.55

activity towards β Pic (Beust et al. 1996) led to estimate that one roughly 1 kilometer-sized body is destroyed in front of the line of sight every day, with temporal fluctuations around one order of magnitude. Assuming that not all FEBs cross the line of sight, we estimate the total number of FEBs evaporated as $N =\sim 10$ per day. Taking kilometer-sized bodies with an average density of 2 g cm^{-3}, assuming that half of their mass is made of metallic ions that are pushed away by radiation pressure, and assuming that the ions spread over an open cone of $\alpha =\sim 30^\circ$ half-opening angle (in order to disperse ions at that latitude), we may estimate the incoming kinetic energy flux F at 100 AU as

$$F = \frac{1}{2}\frac{Nmv^2}{4\pi d^2 \sin\alpha} \sim 0.2\,\mathrm{erg\,cm^{-2}\,s^{-1}}, \quad (1)$$

where $v \simeq 1000\,\mathrm{km\,s^{-1}}$ is the velocity of the incoming ions and m is the average mass of the FEBs. This kinetic energy heats the local H I gas over a distance corresponding to the stopping path of the metallic ions. This depends on the density of the local gas, but we see in Sect. 4 that an H I column density of $\sim 10^{17}$ cm^{-2} is expected to be sufficient to stop the ions over a distance of a few AU.

We thus decided to perform runs of CLOUDY with an extra heating source, with a volume-heating rate (parameter `hextra`) corresponding to the incoming kinetic energy flux deposited over the stopping distance. We performed several runs for hydrogen densities ranging between 10^6 and 10^{10} cm^{-3}. The result listed in Table 1 are for 10^7 cm^{-3}. For other values, the absolute values of the emissions changes, but their relative behaviour remains comparable.

In almost all runs the same line behaviour is reported (Table 1): the Ca II K and H emissions are comparable, the Ca II K emission being slightly stronger; the Na I D_2 emission is typically twice as strong as the Ca II K one, while the Fe II emission is as strong as the Na I one.

This simulation is intended to hold for the gas *out* of the disk mid-plane. The spectrum of β Pic as seen from Earth is known to present stable circumstellar components (Lagrange et al. 1998) due to the gaseous counterpart of the disk. These componenents appear as sharp (~0.1 Å wide) additional absorptions at the bottom of the rotationally broadened photospheric stellar lines.

There is a major difference between ions located in and out of the mid-plane of the disk: the former ones see a stellar spectrum *with* these circumstellar components, while the latter ones see a stellar spectrum *without* these components (because they view the star across the disk, as Earth observers). The ATLAS9 stellar model does not take into account these circumstellar absorptions. Hence we must add them to the model. Unfortunately, adding additional spectral absorptions to the stellar models provided is not a standard procedure for CLOUDY. It is thus not possible to accurately model the emission in the mid-plane of the disk. A first order approximation in order to take these absorptions into account is to apply reduction factors of the stellar flux to ions in the mid-plane of the disk (and only to them). These factors are defined as the ratio of the stellar flux at the bottom of the circumstellar additional absorptions (if present) to the flux at the bottom of the corresponding photospheric lines (or equivalently the top of the circumstellar lines). They are simply measured from observed βPic spectra. We used ESO/HARPS spectra communicated by F. Galland. The factors are listed in Table 1. We note that the circumstellar lines are particularly deep for the Ca II lines.

In order to derive a rough estimate of the line emissions, we may assume that the emission is proportional to the incoming flux. This only applies if the lines are optically thin, but the ratio of 2 between the Na I D_2 and D_1 emission shows that this is the case here. We apply the circumstellar factors of Table 1 to the emission intensities derived from CLOUDY with no circumstellar absorptions. The ratio between Na I and Fe I emissions remains unchanged (thanks to similar circumstellar factors), but the Ca II emissions (in both lines) appears now far weaker (a few hundredth in relative intensity) than the Na I and Fe I ones.

The observational constrains to fulfill (B04) are the following: in the mid-plane, the Ca II emission is small compared to the Na I and Fe I ones; the Na I D_2 to Na I D_1 ratio is close to 2, showing that the emission is optically thin; the emission in the Fe I $\lambda = 3859$ Å line is comparable to that in the Na I D_2 line. Out of the mid-plane, the Ca II emission dominates, but the Fe I line may still be detected, because the wing of the line is much larger than for the Na I lines; the Ca II K to Ca II H ratio is close to one.

Our simple model succeeds in reproducing the emissions in the mid-plane. Out of the mid-plane though, the Na I emission is always stronger than the Ca II one and comparable to the Fe I one. It is thus impossible to simultaneously have a strong Ca II emission, a Fe I emission a few times weaker, and an undetectable Na I emission. The only possibility is to exclude the hypothesis of solar composition.

We come therefore to the following conclusions: 1) for the emission in the mid-plane, the observations can be reproduced assuming solar relative abundances between iron, sodium and calcium; 2) out of the mid-plane, the Fe I and Ca II line intensities can be consistently simulated assuming solar relative abundances; 3) the non-detection of Na I emission out of the mid-plane cannot be explained in these conditions, unless sodium is strongly depleted with respect to solar abundance. The model presented in next section provides a plausible explanation for such sodium depletion.

3. Falling evaporating bodies and high latitude ions

3.1. General features

We propose an origin for the high latitude ions observed by B04. Two facts need to be explained: i) why are there large amounts of gas at 30° above the mid-plane of the disk? ii) why does sodium seem not to be present in this gas? We propose that this high latitude gas could be produced by the Falling Evaporating Bodies (FEBs).

The FEBs are star-grazing bodies that fully evaporate in the vicinity of the star. Dynamically speaking, they are planetesimals that have been extracted from the disk orbiting the star and

driven to high eccentricity orbits. They enter the FEB regime when their periastron reaches a threshold value (∼0.4 AU) that allows the refractory material to evaporate. The details of the evaporation process of the bodies as their periastron decreases down to a few stellar radii are described in Karmann et al. (2003). The bodies start to evaporate at each periastron passage, and their evaporation rate increases as the periastron distance gets smaller. For the sizes considered (∼10 km), the FEBs are fully evaporated when they reach a periastron value $q \simeq 0.15 \pm 0.05$ AU.

Star-grazers may be produced from a disk of planetesimals by planetary perturbations. The most efficient mechanism is the Kozai resonance (Kozai 1962), which concerns bodies that have initial high inclination with respect to the orbital plane of the planetary system. Under secular perturbations, the initially highly inclined body is periodically driven to low inclination, but very eccentric, star-grazing orbits. This mechanism is responsible for most of the sun-grazing bodies reported in the Solar System, such as the Kreutz group (Bailey et al. 1992).

However, the Kozai resonance is due to the secular, circular part of the interaction Hamiltonian with the planet(s). It is therefore invariant with respect to any rotation in the planet's orbital plane. Bodies driven by the Kozai mechanism are thus expected to reach the FEB state with random orbit orientations. This does not match the statistics of the Doppler velocities of the variable spectral events observed, which shows a strong bias towards redshifts. Most of the suspected FEBs share some kind of common preferred periastron orientation range which is not compatible with the Kozai resonance (Beust et al. 1996).

Beust & Morbidelli (1996) proposed that the FEBs could be generated by another mechanism involving mean-motion resonances with at least one major perturbing planet. The secular motion of bodies trapped in a given mean-motion resonance with a planet is usually characterised by coupled oscillations of the semi-major axis and the eccentricity around a median value, but if the planet's orbit is slightly eccentric, these oscillations are superimposed on a long-term drift of the eccentricity that can in some cases bring it to star-grazing values. Yoshikawa (1989) showed that these changes are particularly important for resonances 4:1, 3:1 and 5:2. Beust & Morbidelli (1996) showed that the 4:1 resonance is a potential source of FEBs via this mechanism, and in Thébault & Beust (2001), it was shown that the 3:1 may also contribute to the FEB phenomenon. The planet's eccentricity e' does not need to be very high; $e' \gtrsim 0.05$ is enough, $e' = 0.07$ or 0.1 being typical convenient values. Such eccentricity values are regularly reached by Jupiter due to its secular evolution. This mechanism is close to the one that gave birth to the Kirkwood gaps in the asteroid belt, even if in the latter case, the overlapping of mean-motion resonances with secular resonances considerably enhances the mechanism (Morbidelli & Moons 1993; Moons & Morbidelli 1995; Morbidelli & Moons 1995; Farinella et al. 1994). We cannot exclude this enhancement as being effective in the β Pic system (this would imply the presence of more than one planet), but there is no way to constrain it. We are perhaps witnessing in the β Pic system a process similar to what occurred in the Solar System, as it was of comparable age to β Picś current age.

Due to this mean-motion resonance mechanism, a given body, initially orbiting the star in 3:1 or 4:1 mean-motion resonance with a Jupiter-sized planet, may reach the FEB state within $\sim 10^4$ orbital periods of the planet. Contrary to the Kozai case, the periastron longitudes of the FEBs at high eccentricity are now constrained by that of the perturbing planet, and share some common orientation in closer agreement with the observations. This scenario was numerically tested over a large number of particles (Beust & Morbidelli 2000; Thébault & Beust 2001), using the popular symplectic integration package SWIFT_MVS (Wisdom & Holman 1991; Levison & Duncan 1994). It was shown that the suspected mechanism was able to fairly well match the statistics of the observed FEB velocities, provided the orbit of the perturbing planet adopts a given longitude of periastron with respect to the line of sight. If the disk of planetesimals holds a large enough population of bodies, collisions may help refill the resonance and sustain the FEB activity (Thébault & Beust 2001).

The orbits of the FEB progenitors in the mean-motion resonances are supposed to be roughly coplanar with the plane of the disk. In the simulations of Beust & Morbidelli (2000) and Thébault & Beust (2001), the initial inclinations of the particles with respect to the orbit of the perturbing planet were initially chosen as less than 5° and 3° respectively, in order to mimic the typical distribution within a cold planetesimal disk. During their evolution within the resonance, as long as their eccentricity grows, the inclination of the particles remains small, but as they reach the FEB state close to $e \simeq 1$, their inclination is subject to oscillations of larger amplitude, up to several tens of degrees. This is illustrated in Fig. 1, which shows the secular evolution of the eccentricity and of the inclination of a typical particle trapped in 4:1 resonance with a planet orbiting β Pic. The particle starts at eccentricity $e = 0.05$ and evolves towards the FEB state at $e \simeq 1$ (the peak eccentricity is about 0.998), and then starts a decrease of its eccentricity. Of course the decrease phase is purely fictitious, as a real FEB would be destroyed by the successive periastron passages at peak eccentricity. The inclination, initially set at 2°, remains small for $\simeq 10^5$ yr and then starts oscillations that brings it far above the initial value, up to 40°. This oscillation regime stops after $\sim 2.5 \times 10^5$ yr; it corresponds to the high eccentricity phase, when $e \gtrsim 0.85$. Hence the FEBs may remain within the disk during most of their secular evolution, but finish in the FEB state with inclinations that might bring them significantly out of the disk. The FEB themselves do not have excursions far out of the plane of the disk, because, as we will see below, when their inclination is high, their argument of periastron ω is close to 0° or 180°. This causes the major axis of their orbit to lie roughly in the plane of the disk at the time the inclination is high. As the orbit is very eccentric, the vertical excursion of the particle is limited. This is why this effect, present in the simulations of Beust & Morbidelli (2000) and Thébault & Beust (2001), does not have much influence on the visibility of the FEBs (they need to cross the line of sight to be detected in absorption).

What is true for the parent body is not necessary true for its byproducts. The metallic ions released by the FEBs such as Ca II start to expand radially around the nucleus and stay for a while in a surrounding cloud that enables the FEB to be detected in absorption when it crosses the line of sight; but they are quickly expelled from there by the intense radiation pressure they suffer and then start a free expansion out of the system. This process is extensively described in dedicated simulations in Beust et al. (1990, 1996, 1998). Dynamically speaking, the ratio of the radiation pressure to stellar gravity is a constant (usually noted β) for a given ion or dust grain. This is equivalent to the view that with radiation pressure, the ion feels the gravity of star as if its mass was multiplied by $1-\beta$. For Ca II, $\beta > 1$ ($\beta = 35$), so that the ions feel a negative mass and are strongly repelled by the star. They nevertheless follow a purely Keplerian orbit, namely a hyperbolic repulsive one, similar to the relative motion of two charged particles with charges of the same sign. This orbit is very

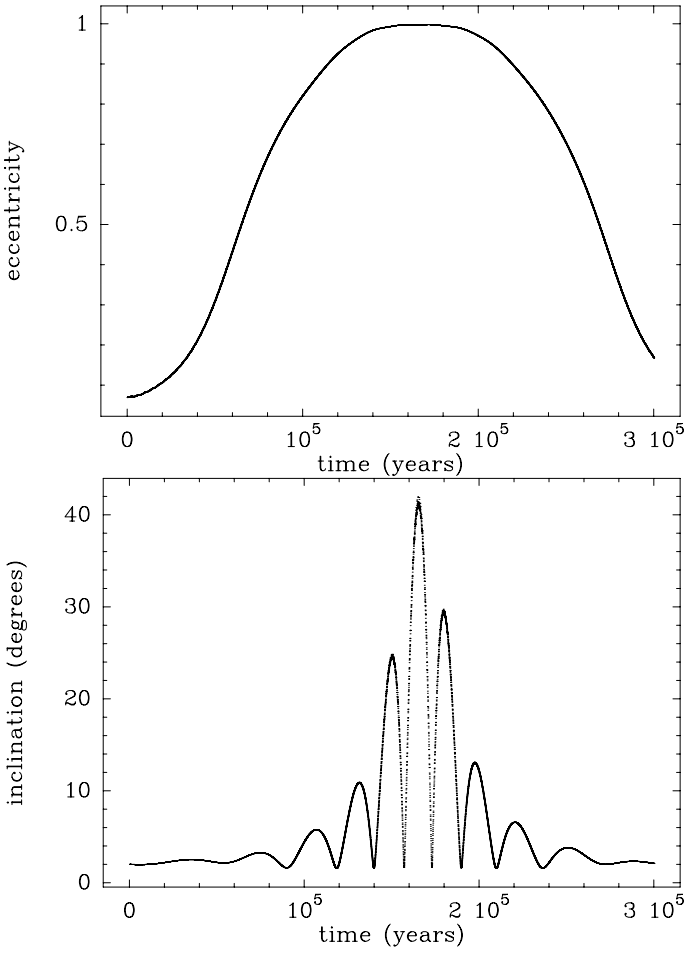

Fig. 1. Temporal evolution of the eccentricity (*top*) and of the inclination (*bottom*) of a typical particle trapped in 4:1 resonance with a planet orbiting β Pic at 10 AU with eccentricity $e' = 0.07$. The planet's mass is 1/1000 of that of the star. The initial eccentricity of the particle is 0.05 and its initial inclination is 2°.

different to that of the parent body. Both orbits share however the *same orbital plane*. Indeed, the ejection velocity of the material escaped from the FEB (typically $\sim 1\,\mathrm{km\,s^{-1}}$; see refs. in Beust et al. 1996) is very small compared to the orbital velocity of the FEB itself at a few stellar radii from the star (typically several hundreds of $\mathrm{km\,s^{-1}}$). The Ca II ions may thus be considered with reasonable accuracy to have the same orbital velocity at ejection time as their parent body. Both Keplerian orbits are very different because of radiation pressure, but they share roughly the same orbital plane. In particular, the Ca II ions keep memory of the orbital inclination of their parent body at ejection time, even if this inclination is large thanks to inclination oscillations in the FEB state. But contrary to the parent body, the orbit of Ca II ions are not confined close to the plane. As explained above, the argument of periastron ω of the parent bodies is close to 0 or 180° in the high inclination state; this forces the FEB to remain close to the mid-plane of the disk. Due to radiation pressure, the shape of the Ca II ions is very different from that of their parent body, and their argument of periastron is not constrained in the same way. If they have a high initial inclination, they may evolve far off the plane of the disk as they escape from the system. If some dense medium is present at a given distance to brake them, they may be detected as an extended emission significantly above the plane such as in the B04 observation. Their detection of Ca II at 33° off the mid-plane could then well correspond to ions that have been produced close to the star by FEBs with similar inclination, and that have freely escaped up to 100 AU before being stopped there.

Then, why should this process only concern Ca II and not the other species detected in emission by B04? Iron and sodium are byproducts of dust sublimation in FEBs like calcium. Contrary to Ca II, Na I and Fe I are quickly photoionized by the star in the FEB environment. Fe II (like Fe I) still undergoes a radiation pressure that overcomes the stellar gravity (Lagrange et al. 1998), so that iron is expected to behave like calcium. However, unless the electronic density is high, as is the case in the vicinity of the mid-plane disk, iron remains predominantly in the Fe II state whose spectral lines were not searched for by B04. Conversely, Na II does not feel any noticeable radiation pressure, so that once produced, the Na II ions keep following the original orbit of the FEB. They may afterwards diffuse slowly in the mid-plane of the disk, but they are not subject to a quick off-plane ejection like the other species. In this context, we thus expect the gas expelled off-plane by this process to contain calcium and iron with solar relative abundances, but no sodium. This matches our analysis of the emission lines.

In the following we detail the theoretical background of the origin of the inclination oscillations of the FEBs in high eccentricity regime, and we show examples from the simulations from Beust & Morbidelli (2000) and Thébault & Beust (2001).

3.2. Three-dimensional motion in mean-motion resonance

The theoretical background for the FEB dynamics in mean-motion resonance is described in Beust & Morbidelli (1996), but restricted to the *planar* case. Here we wish to extend it to three-dimensional motion. We describe the restricted three-body problem, i.e., a problem where a mass-less test particle orbiting a star is perturbed by a planet orbiting the star on an unperturbed Keplerian orbit.

The full analytical analysis is presented in Appendix A. We assume that the particle is locked in a $(p+q)$: p mean-motion resonance with the planet. The resonant motion is usually described by the "critical angle of the resonance" σ (Moons & Morbidelli 1995), with

$$\sigma = \frac{p+q}{q}\lambda' - \frac{p}{q}\lambda - \varpi, \tag{2}$$

where λ is the mean longitude of the particle along its orbit; λ' is the same for the planet; ϖ is the longitude of periastron.

Non-resonant orbits are characterised by a more or less regular circulation of σ, while resonant orbits exhibit libration of σ around a stable position. If the planet's orbit is circular, then the following quantity is a secular constant of motion (Morbidelli & Moons 1993; Moons & Morbidelli 1995):

$$N = \sqrt{(1-\mu)a}\left(\frac{p+q}{p} - \sqrt{1-e^2}\cos i\right), \tag{3}$$

where e is the eccentricity, i is the inclination, and μ is the mass parameter, i.e. the ratio of the planet's mass to the total mass. The inclination oscillations are controlled by this parameter. If the planet's orbit is not circular, then strictly speaking N is no longer constant, but as the planet's eccentricity e' is moderate, its variation is slow.

Considering the circular problem is equivalent to expanding the Hamiltonian $\mathcal{H}$ in powers of e', and retaining only the leading term. The leading (circular) term is responsible for the

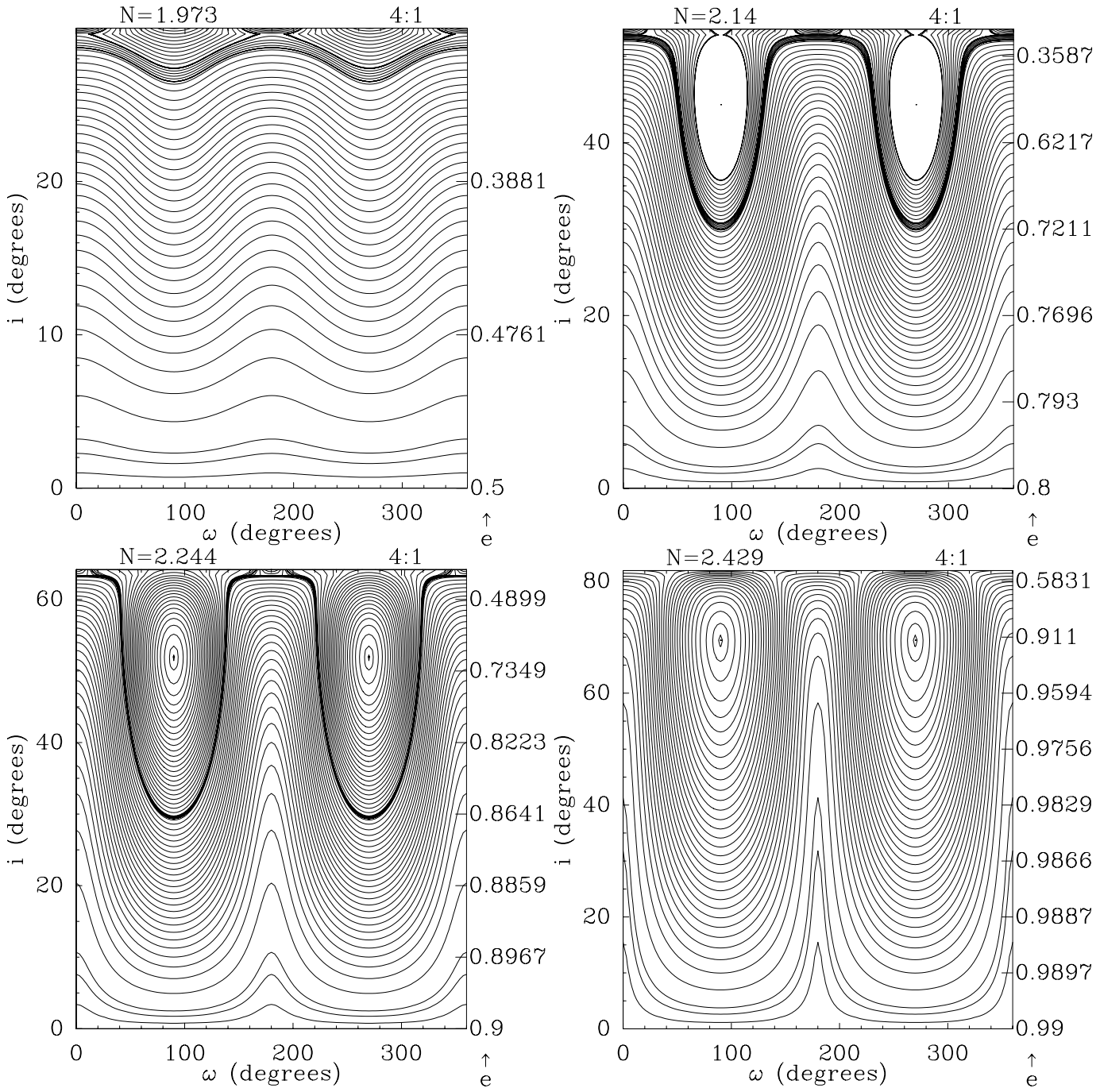

Fig. 2. Level curves of the Hamiltonian $\mathcal{H}$ in the (ω, i) plane for the circular problem, for particles having negligible σ-libration amplitude, for different values of the constant parameter N. The eccentricity scale (denoted "e" on the right of the plots) is related to the inclination scale to the left by the constant value of N.

σ-libration, but also for the inclination oscillations at high eccentricity. The higher order terms in e' cause a slow drift of the N parameter. This drift can drive the particle to high eccentricity, even in the planar problem; this is the way the FEBs are generated.

Finally, the dynamics of the particle is characterised by three time-scales: a first, small one related to the σ-libration; a second, larger one characterising the inclination oscillations; a third, long one describing the secular eccentricity changes from ~0 to ~1. The second time-scale is larger than the first one, but significantly smaller than the third one. Hence during one inclination oscillation, the value of N may be considered as ~ const., which is equivalent to considering the circular problem.

In the circular problem, the secular Hamiltonian $\mathcal{H}$ depends only on the inclination i and on the argument of periastron ω, once the value of N is fixed. It is possible to explore the dynamics just drawing level curves of $\mathcal{H}$ in (ω, i) plane, exactly as done in Beust & Morbidelli (1996). This is done in Fig. 2 for the 4:1 resonance, for 4 different values of N. Instead of giving the value of N, we give a value for the eccentricity and compute the value of N that gives this eccentricity value for $i = 0$. The value of μ was fixed to 0.001 as typical for a Jupiter-sized planet. The value of N is indicated above each plot, and a corresponding

eccentricity scale is given to the right of the plots. The four plots corresponds to eccentricity values at $i = 0$ of 0.5, 0.8, 0.9 and 0.99 (these values appear at the lower right corner of the plots). In all these plots, the eccentricity variation over most of the plot is very moderate. Hence each of these plots should be regarded as a picture of the dynamics in a given eccentricity regime. The plots of Fig. 2 are equivalent to those of Fig. 5 from Morbidelli & Moons (1993) for the 2:1 resonance.

Consider now a given particle trapped in the 4:1 resonance which starts its eccentricity growth. In a low eccentricity regime, like the one for $e = 0.5$ ($N = 1.973$), the inclination remains low while ω circulates. Following a level curve of $\mathcal{H}$, if the inclination is initially low (a few degrees), it undergoes small variations that keep it in the same range. At a higher eccentricity regime, the phase portrait changes. We note in Fig. 2 that two islands of libration for ω appear around $\omega = \pm 90°$. However, these islands of libration do not concern the particles we are considering. Our particles start within the plane of the disk with an inclination that does not exceed a few degrees. Hence the curves they follow are those located *below* the islands of libration. For our particles, ω still circulates, but following the level curves, the inclination i is subject to periodic jumps up to possibly several tens of degrees when ω reaches 0 or π. The higher the eccentricity regime, the higher the inclination jumps. This is the origin of the inclination oscillations reported in the numerical integration.

This dynamics is a resonant version of the Kozai dynamics. In the non-resonant circular restricted problem, the Kozai Hamiltonian describes the secular dynamics of the particle. It is obtained by a double averaging of the original Hamiltonian over the orbital motions of the planet and of the particles (Kinoshita & Nakai 1999). It is well known that this Hamiltonian has a secular constant of motion which is the z-component of the angular momentum (or equivalently $\sqrt{1-e^2}\cos i = \text{const.}$). It is also well known that at high inclination, this Hamiltonian shows two islands of libration in (i, ω) space around $\omega = \pm\pi/2$, and that particles moving in these islands evolve periodically from a high inclination and low eccentricity regime to a low inclination and high eccentricity. This behaviour constitutes the Kozai resonance (Kozai 1962).

The islands of libration in the plots of Fig. 2 describe a Kozai resonance, within a mean-motion resonance. Indeed, as a is fixed the condition $N = \text{const.}$ is exactly equivalent to the Kozai condition $\sqrt{1-e^2}\cos i = \text{const.}$ The FEBs trapped in the 4:1 resonance that evolve at very high eccentricity regimes are concerned by this, but they are *not* trapped into the Kozai resonance, as their argument of periastron ω still circulates, and as they periodically return to $i \simeq 0$. However the Kozai dynamics influences them and causes periodic inclination jumps up to several tens of degrees, even if the initial inclination is low (a few degrees).

3.3. Tests over a large number of bodies

To test the statistical effect of the eccentricity jumps reported, a numerical test over a large number of bodies is necessary. In fact it was not necessary to perform new simulations. We just take the (still available) results of the simulations described in Beust & Morbidelli (2000) and Thébault & Beust (2001). This is illustrated in Fig. 3. In this figure, we consider a typical simulation described in Beust & Morbidelli (2000), with $e' = 0.07$ and $\mu = 0.002$. As described in that paper, the simulation is made over 10^4 particles initially chosen orbiting the star in 4:1 mean motion resonances with the perturbing planets. The initial eccentricities are randomly chosen ≤ 0.1 and the inclinations

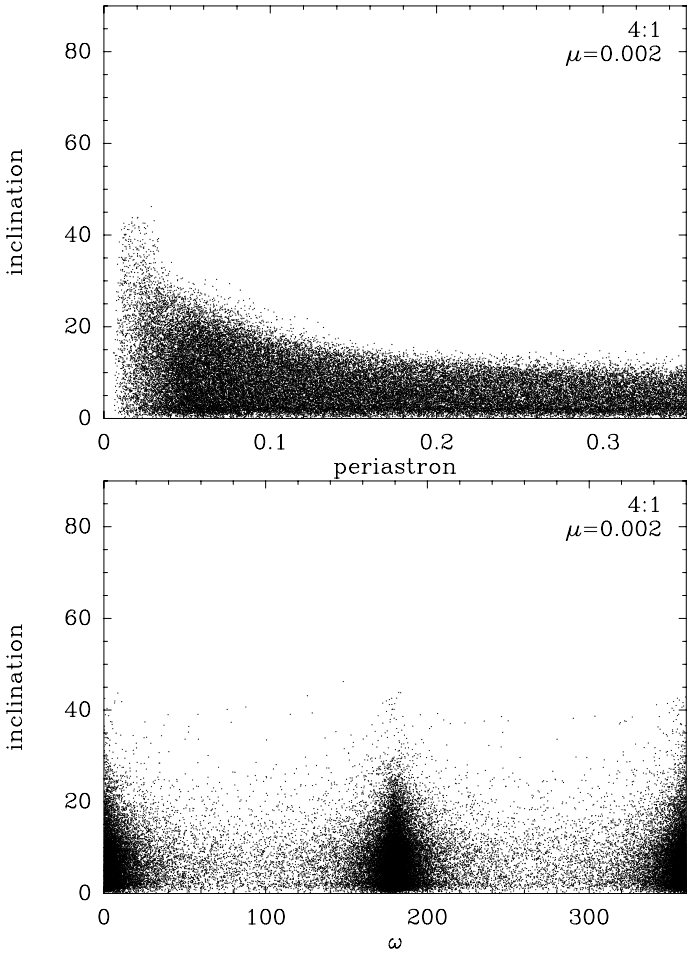

Fig. 3. A statistical test of the inclination oscillation regime for FEBs. These results concern a typical simulation described in Beust & Morbidelli (2000) with $e' = 0.07$ and $\mu = 0.002$. Each dot corresponds to a series of periastron passages of a body that has entered the FEB regime (periastron $\lesssim 0.4$), and that is not yet fully evaporated. *Top plot*: inclination as a function of periastron; *Bottom plot*: inclination as a function of the argument of periastron ω.

$\leq 5°$. In Beust & Morbidelli (2000), it was shown that many of the particles evolve to the FEB regime, and we perform statistics over the expected Doppler velocities when the FEBs cross the line of sight. This statistic appears in agreement with the observational one. In Fig. 3, we display information about the inclinations of the particles when they are in the FEB regime. More specifically, we count all periastron passages for the particles with periastron values less than 0.4 AU (the FEB regime), and that are not yet destroyed by evaporation. Figure 3 shows that the highest inclinations correspond to the smallest periastron values. This is in agreement with the theory outlined above (Fig. 2) which shows that the high inclination oscillations are to be expected in the high eccentricity regime only, i.e. in the FEB regime. Figure 3 also shows that whenever they reach high inclinations, the FEBs assume an argument of periastron close to $\pm\pi/2$. This is in agreement with the theory, and demonstrates the reality of the proposed mechanism. Moreover, the concentration of points close to $\omega \pm \pi/2$ shows that the FEBs spend more time in high inclination regimes than in low regimes. This is confirmed directly by the temporal evolution of the inclination in Fig. 1.

4. Stopping the ions

We showed in the previous section that, due to their inclination oscillations, the FEBs constitute a potential source of Ca II and Fe I ions that may escape far off the disk plane. These ions – being blown away by a strong radiation pressure – should accelerate mostly freely and reach the outer parts of the disk with high velocities, up to $\sim 1000\,\mathrm{km\,s^{-1}}$. However, such velocities would be in sharp contradiction to the observations by B04, where the Ca II ions are found *at rest* with respect to the star, about 116 AU away. This implies that some process is able to efficiently slow down the ions despite the intense radiation pressure they undergo ($\beta = 35$, see above).

This issue was investigated recently by Fernández et al. (2006, hereafter F06) as many metallic species are observed at rest relative to the star despite a strong radiation pressure. They identified three possible braking processes: collisions among ions, collisions with charged ions, and collisions with a neutral gas. Collisions among ions are very efficient (Beust et al. 1989), and the whole plasma tends to behave like a single fluid with a weighted average β. However, F06 show that unless carbon is overabundant, the fluid is still accelerated by the star. Collisions with charged grains are only efficient if the grains are mostly carbonaceous. Moreover, at high latitude in the disk where the Ca II is observed, the density of the dust is low (0.3% of that of the midplane according to the profile given by Fernández et al. 2006). Collisions with neutral gas are conversely a good candidate. F06 showed that a minimum mass of neutral gas of $\sim 0.03\,M_\oplus$ is enough to stop the ions. However, due to the high incoming velocity of the Ca II ions, the basic analytic model must be revised. We detail this below, and conclude that the actual braking is even more effective than in the basic formulation.

4.1. Stopping with gas

Neutral species like H I or He I or even H_2 are not subject to any significant radiation pressure from the star (Lagrange et al. 1998); they may thus stay orbiting in a Keplerian way at some distance from the star. The incoming Ca II ions may then collide into this buffer gas and be slowed down to negligible velocity. This process was also invoked as a way to stop Ca II ions a few AU from the star in order to generate the stable circumstellar Ca II absorption (Lagrange et al. 1998). In that work, we showed that a column density of $\sim 10^{18}\,\mathrm{cm^{-2}}$ is enough to slow down the Ca II ions. Here we investigate whether the same mechanism could also apply to decelerate faster off-plane ions.

The rapid off-plane ions are not stopped at a few AU like those that stay within the plane because they do not encounter any noticeable gaseous medium at their orbital inclination. Why should they be stopped around 116 AU? We must assume that at such a distance, the disk tends to flare. Hence some dilute material could be present at 30° or more in the outer disk while remaining absent in the inner disk. But why 116 AU? This distance corresponds approximately to the location of the power law break-up in the surface brightness radial profile of the disk (Heap et al. 2000). Closer to this threshold, the surface brightness decreases as $r^{-1.1}$, while further away it falls off much more steeply as $r^{-5.5}$. This was interpreted by Augereau et al. (2001) as a consequence of the distribution of planetesimals in the disk. The dust particles are produced by the planetesimals and then scattered into the outer disk by the stellar radiation pressure. The power law break-up at ~ 120 AU is consistent with a planetesimal disk presenting a rather sharp outer edge located at this distance (Augereau et al. 2001). The planetesimals disk appears thus to be truncated at the same distance where the off-plane Ca II ions stop. These facts may be related. The flaring of the disk that we invoke at that distance for stopping the Ca II ions could be due to the perturbations by successive stellar flybys, as was invoked by Larwood & Kalas (2001) as an explanation for asymmetries and arc-like structures in the outer parts of the circumstellar dust disk. But the same mechanism could also be invoked to account for the truncation of the planetesimal disk at the same distance. Further away than 120 AU, the planetesimals are perturbed by stellar flybys, and may not remain in a thin disk. Also the planetesimals themselves may not have had the opportunity to form there. The stellar flybys may have scattered away (and probably in the vertical direction) the initial material from which the planetesimals were expected to form. Thus, the β Pic disk beyond 120 AU could still be in a kind of primordial state where no refractory material condensation would have occurred, with a significant flaring due to stellar flybys.

4.1.1. The analytical induced dipole model and its limitations

We now review the basic mechanism of decelerating by a neutral medium, noting that we depart from the situation described in Lagrange et al. (1998), in two points: i) the volume density of the incoming ions and of the colliding medium is probably much less at 116 AU and 30° inclination than in the plane at a few AU; therefore no significant pressure effect is to be expected and the hydrodynamic description may be dropped; ii) the incoming velocity of the Ca II ions is likely to be much higher. In the limiting case of a free ballistic runaway driven by the radiative pressure of the unobscured star, the resulting velocity is $\sim 1000\,\mathrm{km\,s^{-1}}$, about two orders of magnitude higher than was considered in Lagrange et al. (1998).

A simple collisional decelerating mechanism was initially described in Beust et al. (1989) for moderate velocities. When a charged ion approaches a neutral atom, a dipole is induced on the neutral atom, from which an interaction results between the two particles that may be well described by the potential energy

$$V(r) = \frac{1}{4\pi\epsilon_0}\frac{\alpha q^2}{2r^4}, \tag{4}$$

where α is the polarizability of the atom, r is the interaction distance, and q is the charge of the ion, the other symbols having their usual meaning (McDaniel 1964). The relative motion in this potential cannot be solved exactly, but there is a critical impact parameter b_0 (that depends on the impact velocity v) separating two regimes: for $b > b_0$ there is a minimum approach distance between the particles preventing any close collision; for $b < b_0$ this is not so, and the particles undergo a physical collision (see Appendix B). A fairly correct approximation is then to neglect the effect of the encounter for $b > b_0$, and to consider that the mean impulsion loss by the ion in the physical collision is μv, where μ is the reduced mass. The interaction cross section is then πb_0^2 and the resulting drag force $\boldsymbol{f}$ is opposed to velocity:

$$\boldsymbol{f} = -\mu\pi b_0^2 n v\,\boldsymbol{v}, \tag{5}$$

where n is the number volume density of neutrals. The expression of b_0 (see Appendix B) is

$$b_0 = \left(\frac{1}{4\pi\epsilon_0}\frac{4\alpha q^2}{\mu v^2}\right)^{1/4} \tag{6}$$

Table 2. Values of the critical impact parameter b_0 as a function of the relative velocity v, as computed from Eq. (6) for the Ca II–H I interaction.

v (km s^{-1})	1	10	100	1000
b_0 (nm)	0.785	0.24	0.078	0.024

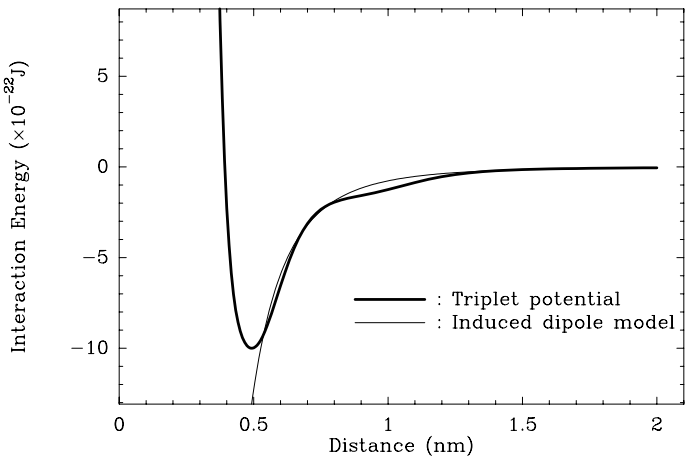

Fig. 4. The ab-initio calculated interaction potential between Ca II and H I (in their ground triplet state) as a function of the mutual distance (fat line), superimposed on the induced dipole potential (thin line).

so that the resulting force is proportional to the velocity: $\boldsymbol{f} = -k\boldsymbol{v}$ with

$$k = n\pi \sqrt{\frac{4\mu\alpha q^2}{4\pi\epsilon_0}}. \quad (7)$$

We confirmed to within 5% this simple analytical approximation of the drag force using the more general numerical treatment described later on.

However this induced dipole regime holds as long as the drift velocity v is not too large. When v grows, b_0 becomes smaller than the physical size of the particles. In this regime the interaction cannot be described any longer as attractive, and it rather approaches a hard sphere regime at shorter range with a constant cross section that does not depend on v. According to Eq. (5), the drag force turns out now to be proportional to v^2 instead of v. Table 2 lists computed values of b_0 for different values of v for the Ca II–H I interaction (the polarisability of H I is 6.7×10^{-31} m^3). We note that as soon as $v \gtrsim 10$ km s^{-1}, this induced dipole model becomes unrealistic because b_0 becomes comparable to or smaller than typical atomic radii. Hence Ca II ions that encounter H I atoms at ~1000 km s^{-1} undergo a collisional interaction that is similar to a hard sphere regime. As the velocity decreases along successive collisions, the interaction finally enters the induced dipole regime. A correct description of the decelerating process of the Ca II ions implies therefore to be able to describe the interaction at *every* velocity, in particular in the intermediate velocity regime between the two above described extremes.

4.1.2. The "smooth sphere" model

In order to have a more coherent description, we introduced a "smooth" sphere approximation based upon a continuous description of the interaction potential $U(r)$ between Ca II and H I as a function of the relative distance r. The interaction originates from a quantum-mechanical interaction at the microscopic level. During a collision, the incoming Ca II and H I particles form an intermediate molecular ion. This molecular complex possess two valence electrons originating from each incoming particle. In a quantum description of the interaction, these two electronic spins recouple to form either a singlet or triplet state with a 3 to 1 probability in favour of the triplet state. However in the case of energetic collisions these input states will interact with various excited states of the same spin multiplicity, leading to numerous inelastic processes that will be sketched in the the next subsection.

Fortunately the ground state triplet state is not expected to be very reactive for moderate collisional energies and could provide a realistic basis for our "smooth" sphere model. Using the ab initio Gaussian 94 package (Frisch et al. 1995) we investigated the triplet input state using a restricted open-shell approach (in order to preserve the total spin). We performed ROMP2 calculations to take into account the electronic correlation and also to some extent the interactions with excited states. We added diffuse and polarization functions on both centers, paying special attention to the proper description of the polarisation of the hydrogen atom. We also performed a population analysis at the Mulliken level to check that charge transfer effects were small (contrary to the singlet state where strong inverse charge transfer effects were found). The resulting triplet potential is plotted in Fig. 4 as a function of r, superimposed on the induced dipole interaction. Our ab-initio potential is consistent with the induced dipole approximation beyond 0.5 nm, but closer to 0.5 nm, it exhibits a repulsive wall providing a smooth transition towards the limiting hard sphere regime.

Let us now take into account this "smooth" sphere potential for a determination of the drag force. Given any interaction potential $U(r)$, the drag force acting on the ion is opposed to the velocity and may be written as

$$\boldsymbol{f} = -4\pi n\mu v \left[\int_0^{+\infty} b \, \sin^2\left(\frac{\chi(b,v)}{2}\right) \mathrm{d}b \right] \boldsymbol{v}, \quad (8)$$

where b is the impact parameter, and $\chi(b, v)$ is the deflection angle due to the encounter corresponding to b and v. $\chi(b, v)$ itself depends on the form of the potential and may be obtained from an integral along the relative motion during the encounter (see Appendix B).

4.1.3. Beyond the "smooth sphere" model: the "inelastic" model

The above expression for the drag force assumes implicitly that the encounters between the ion and the hydrogen atoms are elastic.

On the contrary, energetic collisions are likely to trigger various inelastic processes. For impact velocities in the range 100–1000 km s^{-1}, the energy available in the center of mass is huge, from 50 eV to 5000 eV, and is able to induce a large variety of excitations in both the valence and core electronic space. Beyond the mere electronic excitation of either particles, these energetic collisions can thus trigger a whole range of inelastic and reactive processes including inverse charge transfer, single or multiple electronic ionizations, etc. Collisions with He I or H_2 will be even more energetic due to the larger reduced mass. A detailed theoretical description of all these processes and of their cross sections and branching ratios is beyond the range of the present study. Experimental investigations might provide a better starting point for further studies.

All these inelastic processes will convert a part of the incoming kinetic energy into internal energy of the particles and also, if

ionization occurs, into kinetic energy of the secondary electrons. Of course the internal excitations will mostly decay radiatively and will never be converted back to kinetic energy of the Ca II ions. In addition, the Ca II ions are likely to increase their charge, following either simple or multiple ionization, or inverse charge transfer with H I[1]. Once ionized to Ca III or higher, the calcium ions are expected to recombine to Ca II after a while. But during the time they spend at higher ionization states, they should be decelerated even more effectively, because they no longer feel any significant radiation pressure from the star (as the species under consideration have no strong spectral lines in the visible-UV domain), while the drag force is expected to increase with ionization level.

Moreover, the neutral H I gas, once shocked by the incoming high velocity ions, is expected to be partly ionized by this process. The gas will thus tend to behave like a plasma with a collective dynamical behaviour, resulting in an averaged β ratio, as described by F06. These collective effects should enhance significantly the efficiency of the braking process.

All these inelastic effects will increase the energy loss by the Ca II ions and thus the drag force predicted by the smooth sphere model. Their description is beyond the scope of the present paper. In the following we propose an order-of-magnitude calculation using a very crude model to describe the ionization processes involving collisions between Ca II ions and H I atoms. A simple way to treat possible ionization is to monitor the available kinetic energy $1/2\mu v^2$ before the collision in the inertial referential frame. First we select close collisions for which the interaction departs from the induced-dipole model. Second we consider the opening of successive ionization channels when the energy is augmented. We model the ionization for H I and up to 7 electrons for Ca II, assuming an average energy loss $I_\mathrm{p} = 20\,\mathrm{eV}$ per electron. This loss is supposed to take into account both the extraction energy and the kinetic energy of the expelled electron. The ionization limit of 7 electrons for Ca II is rather arbitrary and includes the 2p shell and the outer 3s electron. The most energetic collisions might rather ionize an inner 1s electron, but this would result in a comparable energy loss because their binding energy is higher, about 150 eV.

In practice, we modify the smooth sphere model with the following prescription. If the available kinetic energy exceeds $k \times I_\mathrm{p}$ with $k \leq 8$ and if the closest approach between the two particles is less than 0.5 nm, the incoming kinetic energy is arbitrarily reduced by $k \times I_\mathrm{p}$. This causes the relative velocity after the encounter v' to be less than the initial velocity v. We define the energy restitution coefficient $e < 1$ as $v' = ev$. This may be written as:

$$\frac{1}{2}mv'^2 = \frac{1}{2}e^2mv^2 = \frac{1}{2}mv^2 - kI_\mathrm{p}. \tag{9}$$

If we assume for simplicity that the deflection angle χ is unchanged with respect to the elastic case, then the expression of the force becomes now

$$\boldsymbol{f} = -2\pi n\mu v\left[\int_0^{+\infty}\left(2e\sin^2\left(\frac{\chi(b,v)}{2}\right)+1-e\right)b\,\mathrm{d}b\right]\boldsymbol{v}. \tag{10}$$

Here the coefficient e is implicitly a function of b and v, as explained above.

The result of the force computation in the various cases is shown in Fig. 5 as a function of the relative velocity v. As in any case the drag force is proportional to the density of the H I medium encountered, showing the force for a unit density medium is enough for comparison purposes. In the induced dipole approximation case, we find as expected $f \propto v$, and we see that this approximation is valid up to $v \simeq 20\,\mathrm{km\,s^{-1}}$. At the higher velocity regime, we have $f \propto v^2$ when the triplet potential is taken into account, corresponding to our smooth sphere regime. When ionization is also taken into account, the non-elastic character of the interactions adds an extra force term to the elastic smooth sphere case. Inelastic effects turns out to be particularly noticeable for $100\,\mathrm{km\,s^{-1}} \lesssim v \lesssim 1000\,\mathrm{km\,s^{-1}}$ (at higher velocity ionization is present but the smooth sphere regime dominates). This velocity regime concerns Ca II ions encountering a H I medium at about 116 AU. Consequently, this order-of-magnitude calculation suggests that a proper inclusion of ionization and other inelastic effects would significantly enhance the effective drag force beyond the predictions of the smooth sphere model.

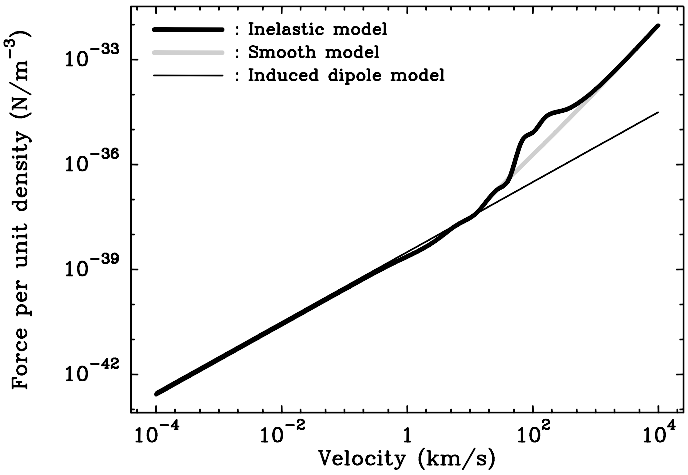

Fig. 5. The drag force on Ca II ions due to a H I medium of unit density ($1\,\mathrm{m^{-3}}$), as a function of the drift velocity v. The thin line corresponds to the induced dipole model, the thick grey line to the smooth model (based upon the triplet potential shown in Fig. 4) and the thick black line to the inelastic model (based upon the combination of the triplet potential and a crude treatment for ionization effects, see text).

4.1.4. Estimate of the required H I column density

Now we have an estimate of the drag force, it is of interest to derive in which conditions the H I medium is able to stop the Ca II ions. Irrespective of the initial velocity, if the medium is dense enough, the ions will always be stopped. The question is to know the amount of H I neutrals required to do this, and more specifically the column density N_s the ions need to cross before being stopped. Let us first consider a simplified case where radiation pressure is not taken into account. The ions arrive at initial velocity v_0 and encounter an H I medium with volume density n. The equation of motion of an ion along its path will be

$$m\frac{\mathrm{d}v}{\mathrm{d}t} = -nF(v), \tag{11}$$

where m is the mass of the ion, and $F(v)$ is the force per unit density shown in Fig. 5. We change the dependent variable t to the integrated encountered column density N ($\mathrm{d}N = nv\,\mathrm{d}t$):

$$mv\frac{\mathrm{d}v}{\mathrm{d}N} = -F(v), \tag{12}$$

[1] In view of our ab-initio investigations, this latter process is expected already to be important at moderate energies for collisions in a singlet electronic state.

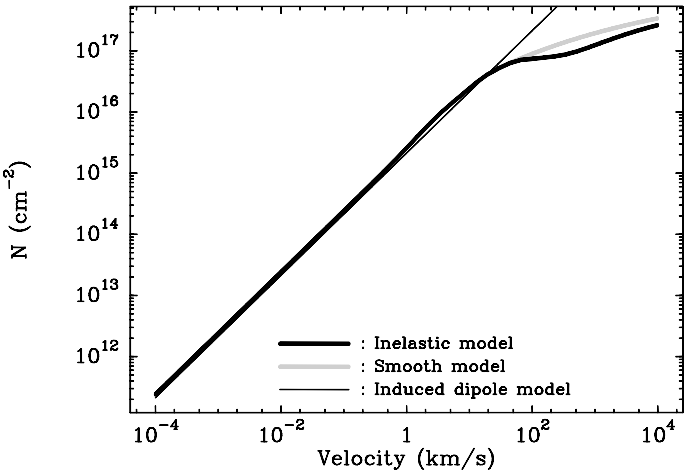

Fig. 6. H I column density necessary to stop Ca II ions, as a function of the initial velocity v_0, as derived from Eq. (13), according to several models (see text). The plotting conventions are the same as in Fig. 5.

from which we immediately derive the integrated column density N_s required to slow the ions from v_0 to 0:

$$N_s = m \int_0^{v_0} \frac{v}{F(v)} \, \mathrm{d}v. \tag{13}$$

Let us now reintroduce the radiation pressure as a constant force P. The equation of motion is

$$m \frac{\mathrm{d}v}{\mathrm{d}t} = P - nF(v), \tag{14}$$

which is equivalent to

$$mv \frac{\mathrm{d}v}{\mathrm{d}N} = \frac{P}{n} - F(v). \tag{15}$$

The ions are now no longer exactly stopped, but rather slowed down to an equilibrium velocity v_{eq} characterised by $nF(v_{eq}) = P$. In practice this terminal velocity is low, so that the ions may be considered as stopped. The radiation pressure P at 116 AU on Ca II ions is $\sim 1.7 \times 10^{-29}$ N (35 times stellar gravity). Let us take the upper limit of 10^{18} cm^{-2} for the hydrogen column density given by Lecavelier des Etangs et al. (2001), spread over a distance d. We derive a ratio

$$\frac{P}{n} = F(v_{eq}) \simeq 2.5 \times 10^{-41} \times d \,(\mathrm{AU})\, \mathrm{N\,m^{-3}}. \tag{16}$$

If we consider as a maximum value for d a few tens of AU, a comparison with Fig. 5 shows that v_{eq} is less than 1 km s^{-1} and that it falls well within the induced dipole regime. This result still holds even if we assume a column density lower by one or even two orders of magnitudes.

Strictly speaking, an infinite column density is required to reach v_{eq}. We should write

$$N_s = m \int_{v_{eq}}^{v_0} \frac{v}{F(v) - F(v_{eq})} \, \mathrm{d}v. \tag{17}$$

As close to v_{eq}, we have $F(v) \propto v$, we derive that the integral diverges logarithmically towards v_{eq}. But reaching a velocity that is of the same order of magnitude as v_{eq} is enough for our purpose. Moreover, for $v \gg v_{eq}$ we have $F(v) \gg F(v_{eq})$, so that $F(v_{eq})$ can be neglected in Eq. (17). Finally, Eq. (13) turns out to be a good estimate for N_s even in the presence of radiation pressure. This is due to the fact that the terminal velocity v_{eq} is very low.

N_s as given from Eq. (13) is plotted on Fig. 6 as a function of the initial velocity, for the various interaction models considered. As expected, in the induced dipole regime, we have $N_s \propto v_0$, but at higher velocity, N_s is reduced by several orders of magnitude with respect to that crude estimate. The smooth sphere model causes N_s to stay below a few 10^{17} cm^{-2} (asymptotically $N_s \propto \ln v_0$). With $v_0 = 1000$ km s^{-1}, we predict $N_s \simeq 10^{17}$ cm^{-2}. This is one order of magnitude below the upper limit to the H_2 column density towards β Pic (Lecavelier des Etangs et al. 2001). As suggested by our inelastic model, the inclusion of inelastic effects would further lower the required column density. Moreover, the collective effects decribed by F06, due to partial ionization of the neutral gas, are expected to enhance the braking process. N_s could thus be even less than the value we derive.

Hence we stress that the model we present here provides a plausible mechanism for stopping the Ca II ions at 100 AU from β Pic, in order to render them detectable in emission.

4.2. Stopping with a magnetic field

Another natural interaction ions that may be subjected to is the influence of a magnetic field $\boldsymbol{B}$ they would encounter at 100 AU. In the presence of a magnetic field, the equation of motion of an ion is

$$m \frac{\mathrm{d}\boldsymbol{v}}{\mathrm{d}t} = \boldsymbol{P} + q\,\boldsymbol{v} \times \boldsymbol{B}, \tag{18}$$

where $\boldsymbol{P}$ is the radial radiation pressure. Let us consider for simplicity that $\boldsymbol{P}$ is constant (the ions are supposed to be stopped over a short distance), as is $\boldsymbol{B}$. The equation of motion has a well-known analytical solution. Introducing a referential frame $(\mathrm{O}x, \mathrm{O}y, \mathrm{O}z)$ where $\boldsymbol{B} \parallel \mathrm{O}z$ and $\boldsymbol{P}$ lies in the $x\mathrm{O}z$ plane, and the angle ϕ between $\boldsymbol{P}$ and the $x\mathrm{O}y$ plane, the solution may be described in that referential as

$$\begin{cases} v_x &= \omega_g \cos\phi \left[R\cos(\omega_g t) + L\sin(\omega_g t) \right] \\ v_y &= \omega_g \cos\phi \left[L(\cos(\omega_g t) - 1) - R\sin(\omega_g t) \right] \\ v_z &= \omega_g \sin\phi \left(L\omega_g t + R \right). \end{cases} \tag{19}$$

The ion is supposed to initially move radially at velocity v_0. Here $\omega_g = qB/m$ is the gyromagnetic frequency; $R = mv_0/qB$ is the gyromagnetic radius associated with the velocity v_0; L is defined as $P = mL\omega_g^2$, i.e., it is a characteristic length associated with the strength of the radiation pressure. The motion perpendicular to the field is a cycloid-like motion, i.e., a combination of a circular motion of radius $\rho = \sqrt{R^2 + L^2}\cos\phi$ at frequency ω_g and of a linear drift at velocity $L\omega_g \cos\phi$. The motion parallel to the field is uniformly accelerated by the radiation pressure. It is important to note that here, contrary to the neutral drift model, the velocity does not reach an asymptotic value. If the field is not perpendicular to $\boldsymbol{P}$ ($\sin\phi \neq 0$) the velocity even increases continuously. But even if $\sin\phi = 0$ the motion in the $x\mathrm{O}y$ plane is still cycloid-like, and the modulus of velocity undergoes a periodic modulation of amplitude $2\rho\omega_g$. Let us now consider a typical magnetic field of 1 μG, at 116 AU from the star, and $v_0 = 1000$ km s^{-1}. We derive $L = 3 \times 10^{-9}$ AU and $R = 0.028$ AU. Hence $L \ll R$ (i.e., the Lorentz force dominates the radiation pressure), and $\rho \simeq R$. This yields $2\rho\omega_g \simeq 2v_0 = 2000$ km s^{-1}. The ions turn out to have velocities relative to the star randomly distributed over a range of 2000 km s^{-1}. Even if the ions do not drift away significantly, their residual velocity range remain far above the spectral resolution of the instruments, and they should not be observed as a

single line at rest with respect to the star. In consequence, this purely magnetic deceleration model cannot account for the observations.

4.3. Combining gas drag and magnetic field

We investigate the possible combination of the two preceding models, i.e., combining a magnetic field and gas drag. The equation of motion is now

$$m\frac{\mathrm{d}\boldsymbol{v}}{\mathrm{d}t} = \boldsymbol{P} + q\,\boldsymbol{v}\times\boldsymbol{B} + \boldsymbol{f}, \tag{20}$$

where $\boldsymbol{f}$ is the gas drag force. In the general case where $\boldsymbol{f}$ is given by Fig. 5, this equation cannot be solved analytically, but at low velocity in the induced dipole regime where $\boldsymbol{f} = -k\boldsymbol{v}$, the differential system remains linear and may be solved exactly after a somewhat lengthy but straightforward algebra. Keeping the definitions and notations of the preceding sections, the solution is

$$\left\{\begin{array}{rcl} v_x &=& \cos\phi\left[(R\omega_\mathrm{g} - L\omega_\mathrm{r})\cos(\omega_\mathrm{g}t) + L\omega_\mathrm{g}\sin(\omega_\mathrm{g}t)\right]\mathrm{e}^{-\omega_\mathrm{r}t} \\ && \qquad + L\omega_\mathrm{r}\cos\phi \\ v_y &=& \cos\phi\left[L\omega_\mathrm{g}\cos(\omega_\mathrm{g}t) + (L\omega_\mathrm{r} - R\omega_\mathrm{g})\sin(\omega_\mathrm{g}t)\right]\mathrm{e}^{-\omega_\mathrm{r}t} \\ && \qquad - L\omega_\mathrm{g}\cos\phi \\ v_z &=& \sin\phi\,\dfrac{R\omega_\mathrm{r}\omega_\mathrm{g} - L(\omega_\mathrm{r}^2+\omega_\mathrm{g}^2)}{\omega_\mathrm{r}}\,\mathrm{e}^{-\omega_\mathrm{r}t} + L\sin\phi\,\dfrac{\omega_\mathrm{r}^2+\omega_\mathrm{g}^2}{\omega_\mathrm{r}}. \end{array}\right. \tag{21}$$

Here ω_g and R are defined as above, $\omega_\mathrm{r} = k/m$ is a frequency characterising the drag force; L is now defined as $P = mL(\omega_\mathrm{r}^2+\omega_\mathrm{g}^2)$. The motion is still combination of a circular motion and a linear drift, but the circular motion is damped exponentially at frequency ω_r, so that the velocity assumes an asymptotic value like in the gas drag case without a magnetic field.

Taking now the numbers given above, and considering a typical expected neutral density of $10^4\,\mathrm{cm}^{-3}$ (a column density of $\sim 10^{17}\,\mathrm{cm}^{-2}$ over ~ 1 AU), we derive $\omega_\mathrm{g} \simeq 2.4\times10^{-4}\,\mathrm{s}^{-1}$ and $\omega_\mathrm{g}/\omega_\mathrm{r} \simeq 78$. Hence the exponential damping is a slower process than the gyromagnetic motion. As $\omega_\mathrm{r} \ll \omega_\mathrm{g}$, the numerical value of L is virtually unchanged with respect to the preceding definition, and we still have $L \ll R$. After damping, the ions have a terminal velocity with respect to the gas given by

$$v_\mathrm{t} = \frac{L(\omega_\mathrm{r}^2+\omega_\mathrm{g}^2)}{\omega_\mathrm{r}}\sqrt{\frac{\omega_\mathrm{r}^2+\omega_\mathrm{g}^2\sin^2\phi}{\omega_\mathrm{r}^2+\omega_\mathrm{g}^2}} = \frac{P}{k}\sqrt{\frac{\omega_\mathrm{r}^2+\omega_\mathrm{g}^2\sin^2\phi}{\omega_\mathrm{r}^2+\omega_\mathrm{g}^2}} \simeq \frac{P}{k}\,\sin\phi. \tag{22}$$

P/k is the equilibrium velocity v_eq given by Eq. (16) in the gas drag case, in the case of the induced dipole regime. Hence the terminal velocity v_t appears in any case less than v_eq. It can even reach zero if the field is perpendicular to the initial motion.

Finally, the net result of the interaction is a deceleration of the ions that is similar to the non-magnetic case. The terminal velocity is comparable (or even less), and it is reached within the same characteristic time $1/\omega_\mathrm{r} = m/k$. The only difference concerns the path of the ions. When no magnetic field is present, the motion of the ions is linear and they are stopped after having encountered a column density of $10^{17}\,\mathrm{cm}^{-2}$, i.e., 0.7 AU with $n = 10^4\,\mathrm{cm}^{-3}$. With a magnetic field, the path is no longer linear. When $\phi = 0$, the radial extent of the spiral motion of the ions before being stopped is $\simeq 2\rho'$ at $t = 0$, i.e., $\simeq 2R$. With the values quoted above, this is about 0.055 AU; with $n = 10^4\,\mathrm{cm}^{-3}$, the corresponding column density is $\sim 8.3\times10^{15}\,\mathrm{cm}^{-2}$. Hence the ions appear to be stopped over a much shorter distance. This is only due to the fact that the motion is not linear. As the ions spiral into the quoted distance, they encounter the required $10^{17}\,\mathrm{cm}^{-2}$ to stop them, but not in a linear fashion, rather inside a box of smaller dimensions.

The magnetic field appears then as an additional source of deceleration for the ions, but the gas drag remains unavoidable. Our conclusion is then that a magnetic field may be invoked as a refinement to the model, but that it is not necessary, the basic process of deceleration remaining the gas drag.

The main issue concerning the magnetic field should be its sudden presence around 100 AU. Why should a magnetic field of 1 μG appear there while not present closer to the star? The only possibility is to invoke a kind of heliopause. β Pictoris is the only normal A type star for which a chromospheric activity was detected by Bouret et al. (2002). These authors derive a mass loss rate $\dot{M} = 2.5\times10^{-14}\,M_\odot\,\mathrm{yr}^{-1}$, with a terminal velocity of $200\,\mathrm{km\,s}^{-1}$. Roughly speaking, the suspected heliopause should be expected where the magnetic pressure $B^2/2\mu_0$ of the surrounding galactic field equals the kinetic pressure of the wind. With the values of Bouret et al. (2002) and $B = 1\,\mu$G, it occurs at 529 AU; alternatively, if we want this to occur at 116 AU, a galactic field of 4.5 μG is required. Inside this cavity, the field would be radial and have no effect on the motion of the ions. These are likely values, so that the possibility cannot be excluded.

5. Conclusion

The presence of metallic ions at fairly high latitude over the midplane of the β Pic circumstellar disk, as observed by B04, can be very well explained as a consequence of the FEB process. Whenever the evaporating bodies enter the star grazing regime, they are subject to inclination oscillations up to $\sim$30–40°. The Ca II ions released by the FEB during this phase start a free, almost radial expansion pushed by a strong radiation pressure, keeping track of their initial orbital inclination. Iron is also concerned by this process, and we expect Fe I ions to be present at high latitude together with Ca II. The Fe I in the data of B04 is not null where Ca II is detected. We nevertheless explain in our emission line analysis that, unless the electronic density is high, the Fe I emission is expected to be weaker than the Ca II one, thanks to a predominant ionization of Fe I into Fe II.

This process does not concern Na I ions because, once produced by the FEBs, they are quickly photoionized into Na II and subsequently no longer experience any noticeable radiation pressure. Hence we explain the absence of Na I emission at high latitude.

Blown away by strong radiative pressure from the star, the Ca II ions reach the distance of $\sim$100 AU in about 1 yr with final velocities of $\sim 1000\,\mathrm{km\,s}^{-1}$. They need thus to be slowed down in order to gather at the star velocity and to form an observable line. This can be achieved if the ions encounter at that distance a neutral gaseous medium, in agreement with the conclusions of F06. A rough estimate of the incoming ion flux due to the FEB activity shows that it can account for the necessary heating source to render the lines observable.

In addition to the induced dipole drag force considered by F06, we estimated additional braking effects arising for rapid collisional velocities. If we consider the effect of repulsive core and inelastic interactions discussed in Sects. 4.1.2 and 4.1.3, a column density of $10^{17}\,\mathrm{cm}^{-2}$ of H I is sufficient to stop the ions

over a distance of a few AU. The inelastic model we introduced is probably very crude, but it is still likely to underestimate the effective drag force. Therefore irrespective of the detailed description of the interaction processes, the required column density remains below the upper detection limit of 10^{18} cm^{-2} given by Lecavelier des Etangs et al. (2001). Following F06, it should even be less if we took into account the collective plasma behaviour due to partial ionization of the neutral gas into account. Conversely, due to the high latitude over the dust disk, we do not expect collisions with dust grains (invoked by F06 as a possible braking mechanism) to play a significant role in the decelerating process of the incoming ions.

We also investigate the possible role of a magnetic field in stopping the ions. While the sole action of a magnetic field is unable to sufficiently slow down the ions, magnetic interactions provide an additional braking process to the basic gas drag model invoked. Combining gas drag and magnetic interactions can thus be a very efficient way to decelerate the ions, still reducing the requirements on the neutral gas density by an order of magnitude. This nevertheless constitutes a refinement of the model, as gas drag in itself is sufficient to account for current observational constraints.

The key parameter in this model is the distance ($\sim$100 AU) at which the ions are stopped. In the gas drag model, we need to assume that no neutral medium is present at 30° inclination up to that distance, so that the ions can freely expand radially, and that they suddenly encounter some medium there. This would mean that the disk begins to significantly flare at that distance. As explained above, this distance corresponds also to the expected outer edge of the planetesimal disk that produces the dust, according to Augereau et al. (2001). These two facts are probably related.

Our conclusion is thus that the proposed scenario is plausible. Another important issue in this study is the number of Ca II or Fe I ions necessary to account for the observations of B04. It cannot be determined easily even if we may estimate the incoming flux, as it depends highly on the time the ions stay within the neutral medium before diffusing away, and subsequently on the small asymptotic drift velocity they reach. If a magnetic field plays a role, this velocity is expected to be significantly lower than without a field; hence the ions should drift more slowly across the neutral medium. At a given epoch, for the same incoming Ca II flux more ions are therefore expected to be trapped in the neutral gas if magnetic forces are active than in the opposite case. This is why deriving an incoming Ca II flux in order to compare to the expected number of FEBs is very imprecise. This could be the purpose of future investigations. Fortunately the uncertainties in the proposed deceleration models are irrelevant here, because once the ions have been decelerated, the analytical induced dipole model should be valid.

Our estimate of the incoming ions flux due to FEB activity (Sect. 2) is very rough, mainly because the FEB activity itself is hard to constrain. Moreover, we expect this activity to be time-variable, as changes have been observed between various observing epochs (Tobin et al. 2004). As the emission lines are supposed to depend on this flux (via the heating source), we expect the strength of the emission lines to present temporal variations (at least those at high latitude). It would thus be of interest to initiate a follow-up of these lines to check for temporal changes.

The FEB scenario is reinforced by the present analysis. The off-plane presence of some metallic species, and the absence of some others, appear as a natural consequence of the FEB scenario and of the mean-motion resonance model with a giant planet. This strengthens our view of the β Pic system as a young planetary system.

Acknowledgements. All the computations presented in this paper were performed at the Service Commun de Calcul Intensif de l'Observatoire de Grenoble (SCCI). Comments by our referee, V. Grinin, and by the Editor, M. Walmsley, inspired the emission model presented in Sect. 2.

References

Artymowicz, P. 1997, Ann. Rev. Earth Planet. Sci., 25, 175
Augereau, J.-C., & Papaloizou, J. C. B. 2004, A&A, 414, 1153
Augereau, J.-C., Nelson, R. P., Lagrange, A.-M., Papaloizou, J. C. B., & Mouillet, D. 2001, A&A, 370, 447
Bailey, M. E., Chambers, J. E., & Hahn, G., 1992, A&A, 257, 315
Barrado y Navascués, D., Stauffer, J. R., Song I., & Caillault, J.-P. 1999, ApJ, 520, L123
Beust, H., & Morbidelli, A. 1996, Icarus, 120, 358
Beust, H., & Morbidelli, A. 2000, Icarus, 143, 170
Beust, H., Lagrange-Henri, A.-M., Vidal-Madjar, A., & Ferlet, R. 1989, A&A, 223, 304
Beust, H., Lagrange-Henri, A.-M., Vidal-Madjar, A., & Ferlet, R. 1990, A&A, 236, 202
Beust, H., Lagrange, A.-M., Plazy, F., & Mouillet, D. 1996, A&A, 310, 181
Beust, H., Lagrange, A.-M., Crawford, I. A., et al. 1998, A&A, 338, 1015
Bouret, J.-C., Deleuil, M., Lanz, T., et al. 2002, A&A, 390, 1049
Brandeker, A., Liseau, R., Olofsson, G., & Fridlund, M. 2004, A&A, 413, 681
Farinella, P., Froeschlé, Ch., Froeschlé C., et al. 1994, Nature, 371, 315
Ferland, G. J., Korista, K. T., Verner, D. A., et al. 1998, PASP, 110, 761
Ferlet, R., Hobbs, L. M., & Vidal-Madjar, A. 1987, A&A, 185, 267
Fernández, R., Brandeker, A., & Wu, Y. 2006, ApJ, 643, 509
Heap, S. R., Lindler, D. J., Lanz, T. M., et al. 2000, ApJ, 539, 435
Hobbs, L. M., Vidal-Madjar, A., Ferlet, R., Albert, C. E., & Gry, C. 1985, ApJ, 293, L29
Jolly, A., McPhate, J. B., Lecavelier, A., et al. 1998, A&A, 329, 1028
Kalas, P., & Jewitt, D. 1995, AJ, 110, 794
Karmann, C., Beust, H., & Klinger, J. 2003, A&A, 409, 347
Kinoshita, H., & Nakai, H. 1999, Celest. Mech., 75, 125
Kozai, Y. 1962, AJ, 67, 591
Kurucz, R. L. 1991, in Stellar Atmospheres-Beyond classical Models, ed. A. G. Davis Philip, A. R. Upgren, & K. A. Janes (L. Davis Press, New-York: Schenectady), 441
Lagrange, A.-M., Plazy, F., Beust, H., et al. 1996, A&A, 310, 547
Lagrange, A.-M., Beust, H., Mouillet, D., et al. 1998, A&A, 330, 1091
Larwood, J. D., & Kalas, P. G. 2001, MNRAS, 323, 402
Lecavelier des Etangs, A., Vidal-Madjar, A., & Ferlet, R. 1996, A&A, 307, 542
Lecavelier des Etangs, A., Vidal-Madjar, A., Roberge, A., et al. 2001, Nature, 412, 706
Levison H. F., & Duncan M. J. 1994, Icarus, 108, 18
McDaniel, E. W. 1964, in Collision phenomena in ionized gases (John Wiley & Sons)
Moons, M. 1994, Celest. Mech. Dyn. Astron., 60, 173
Moons, M., & Morbidelli, A. 1995, Icarus, 114, 33
Morbidelli, A., & Moons, M. 1993, Icarus, 102, 316
Morbidelli, A., & Moons, M. 1995, Icarus, 115, 60
Mouillet, D., Larwood, J. D., Papaloizou, J. C. B., & Lagrange, A.-M. 1997, MNRAS, 292, 896
Olofsson, G., Liseau, R., & Brandeker, A. 2001, ApJ, 563, L77
Ortega, V. G., de la Reza, R., Jilinski, E., & Bazzanella, B. 2004, ApJ, 609, 243
Petterson, O. K.L., & Tobin, W. 1999, MNRAS, 304, 733
Smith, B., & Terrile, R. 1984, Science, 226, 1421
Thébault, P., & Beust, H. 2001, A&A, 376, 621
Thébault, P., Augereau, J. C., & Beust, H. 2003, A&A, 408, 775
Thi, W. F., Blake, G. A., van Dishoeck, E. F., et al. 2001, Nature, 409, 60
Tobin, W., Barnes, S. I., & Pollard, K. R. 2004, ASP Conf. Proc., 321, ed. J.-P. Beaulieu, A. Lecavelier des Etangs, & C. Terquem, 327
Vidal-Madjar A., Lagrange-Henri, A.-M., Feldman, P. D., et al. 1994, A&A, 290, 245
Weinberger, A. J., Becklin, E. E., & Zuckerman, B. 2003, ApJ, 584, L33
Wisdom, J., & Holman, M. 1991, AJ, 102, 1528
Yoshikawa, M. 1989, A&A, 213, 436
Zuckerman, B., Song, I., Bessell, M. S., & Webb, R. A. 2001, ApJ, 562, L87
Frisch, M. J., Trucks, G. W., Schlegel, H. B., et al. 1995, Gaussian 94, Revision E.2 (Pittsburgh PA: Gaussian Inc.)

Online Material

Appendix A: Mean-motion resonance theory

We describe here the non-planar restricted three-body problem, with a mass-less test particle orbiting a star, and perturbed by a planet orbiting the star. The position vectors of the particle and the planet relative to the star are noted $\boldsymbol{r}$ and $\boldsymbol{r'}$ respectively. As usual, we call μ the ratio of the mass of the planet to the total mass of the system m. We assume that $\mu \ll 1$. In this framework, the Hamiltonian of the problem is (see, for instance Morbidelli & Moons 1993)

$$\mathcal{H}_0 = -\frac{1-\mu}{2a} - \mu\left(\frac{1}{|\boldsymbol{r}-\boldsymbol{r'}|} - \frac{\boldsymbol{r}\cdot\boldsymbol{r'}}{r'^3}\right), \tag{A.1}$$

where a is the osculating semi-major axis of the orbit of the particle. Here the Hamiltonian has been normalised by the constant factor $\mathcal{G}m$, where $\mathcal{G}$ is the constant of gravitation. The usual way is then to start from the classical canonically conjugate Delaunay variables:

$$\begin{aligned} &M,\ L = \sqrt{(1-\mu)a} \\ &\omega,\ G = L\sqrt{1-e^2} \\ &\Omega,\ H = G\cos i. \end{aligned} \tag{A.2}$$

Here M is the mean anomaly along the orbit of the particle, ω is its argument of periastron, Ω its longitude of ascending node, e its eccentricity and i its inclination with respect to the orbital plane of the planet.

We assume here that the particle is locked in a $(p+q)$: p mean-motion resonance with the planet. It is then of interest to introduce new canonically conjugate angle-action variables that take into account the resonance:

$$\begin{aligned} &\sigma = \frac{p+q}{q}\lambda' - \frac{p}{q}\lambda - \varpi, \quad S = L - G \\ &\sigma_z = \frac{p+q}{q}\lambda' - \frac{p}{q}\lambda - \Omega, \quad S_z = G - H \\ &-\nu = \frac{p+q}{q}\lambda' - \frac{p}{q}\lambda, \qquad N = \frac{p+q}{p}L - H. \end{aligned} \tag{A.3}$$

The modified Hamiltonian is

$$\mathcal{H} = \mathcal{H}_0 - \frac{p+q}{p}L. \tag{A.4}$$

Here $\lambda = M+\omega+\Omega$ is the mean longitude of the particle along its orbit; λ' is the same for the planet; $\varpi = \omega + \Omega$ is the longitude of periastron. These variables are introduced by Morbidelli & Moons (1993) and Moons (1994). The angle σ is often called the "critical angle of the resonance" (Moons & Morbidelli 1995). Resonant orbits are characterised by a libration of σ around a stable position.

The secular dynamics is investigated by performing a time-averaging of $\mathcal{H}$ over the only remaining fast variable, λ'. If the orbit of the planet is circular, then the averaged Hamiltonian turns out to be independent of ν, showing that N is a secular constant of motion (Morbidelli & Moons 1993; Moons & Morbidelli 1995). This can be checked with explicit expressions, but this arises from the d'Alembert rules: σ and σ_z are independent of any axis rotation within the orbital plane of the planet, while this is not the case for ν. If the planet's orbit is circular, the whole Hamiltonian is expected to be invariant for any rotation in that plane, and should consequently not depend on ν. In that case, the Hamiltonian has two degrees of freedom. If we restrict our study to *planar* motion, then the variables σ_z and S_z disappear and the averaged Hamiltonian is integrable. The secular motion is characterised, together with the librations of σ, by coupled oscillations in the (a, e) plane around the equilibrium value, along a curve N = const. This dynamics is described for many specific resonances by Morbidelli & Moons (1993); Moons & Morbidelli (1995).

If the orbit of the planet is not circular, the action N is no longer constant. It is thus able to evolve, but on a much longer time-scale than the main librations of σ. Therefore, on a short time-scale the oscillations in (a, e) space are preserved, but on a longer time-scale, the value of N is subject to changes that may drive the eccentricity to high values. As quoted by Yoshikawa (1989), these changes are particularly important for resonances 4:1, 3:1 and 5:2. Beust & Morbidelli (1996) showed that the 4:1 resonance is a potential source of FEBs via this mechanism, and Thébault & Beust (2001) show that the 3:1 resonance may also contribute to the FEB phenomenon.

If we return to the spatial problem and give an initially moderate inclination to the particle, these dynamics are preserved. In fact all the simulations presented in Beust & Morbidelli (2000) and Thébault & Beust (2001) were three-dimensional, and the behaviour reported was in perfect agreement with the planar description. However, the planar model does not describe the inclination oscillations observed whenever the eccentricity reaches high values. In order to explain them, we must consider the spatial problem as a whole.

To further study the problem, Morbidelli & Moons (1993) introduce the following canonically conjugate action-angle variables:

$$\begin{aligned} &\psi_\sigma = \frac{2\pi}{T_\sigma}, && J_\sigma = \frac{1}{2\pi}\oint S\ \mathrm{d}\sigma \\ &\psi_z = \sigma_z - \rho_z(\psi_\sigma, J_\sigma, J_z, J_\nu), && J_z = S_z \\ &\psi_\nu = \nu - \rho_\nu(\psi_\sigma, J_\sigma, J_z, J_\nu), && J_\nu = N, \end{aligned} \tag{A.5}$$

where T_σ is the libration period of σ, t is the time, and J_σ is computed over one libration cycle of σ. ρ_ν and ρ_z are functions that are periodic with zero average in ψ_σ.

We are interested in the *secular* dynamics inside the resonance; hence we perform a second averaging of $\mathcal{H}$ over ψ_σ. The function ρ_ν and ρ_z disappear then and J_σ is a new secular constant of motion. J_σ is the normalised area enclosed by the libration trajectory in (S, σ) space. It is close to the amplitude of the libration in σ. Thus in the non-circular problem, the value of N may change, but the amplitude of the libration is roughly preserved. Curves of J_σ = const. for various resonances are given in Morbidelli & Moons (1993); Moons & Morbidelli (1995).

The inclination oscillations are related to the coupled evolution of ψ_z and J_z. This is not easy to describe in the general case as the Hamiltonian $\mathcal{H}$, even averaged over ψ_σ, is still not integrable, as depending on several angles, and because the relationship between ψ_z, ν and J_σ and the usual orbital elements is not straightforward. A convenient way to investigate the dynamics is to restrict the study to the case $J_\sigma = 0$, i.e., orbits with negligible libration amplitude. In this case, the semi-major axis a assumes a fixed value (the pericentric equilibrium) close to the unperturbed value of the resonance; σ also is fixed to an equilibrium value σ_0. The value of σ_0 depends on the resonance under consideration. It is then easy to show that under these conditions $\psi_z = \sigma_z = \sigma_0 + \omega$. This method of considering zero amplitude libration was used in Beust & Morbidelli (1996) to draw Hamiltonian maps in the planar problem.

If we consider the circular (but non-planar) problem, the secular Hamiltonian $\mathcal{H}$, once averaged over ψ_σ, has only one degree on freedom left. It is a function of ψ_z and J_z, or alternatively of i and ω, the constant value of N acting as a parameter.

Appendix B: The drag force theory

Given the interaction potential $U(r)$ (the potential energy being $\mu U(r)$), the encounter between a Ca II ion and an H I atom may be studied using energy and momentum conservation:

$$\frac{1}{2}\left(\dot{r}^2 + r\dot{\theta}^2\right) + U(r) = \frac{1}{2}v^2; \tag{B.1}$$

$$r^2\dot{\theta} = bv, \tag{B.2}$$

where the relative motion is described by its polar coordinates (r, θ), v is the incoming velocity, b is the impact parameter, and $\dot{r}$ and $\dot{\theta}$ are as usual shorthands for $\mathrm{d}r/\mathrm{d}t$ and $\mathrm{d}\theta/\mathrm{d}t$. Eliminating $\dot{\theta}$ leads to the radial equation

$$\dot{r}^2 = -2U(r) + v^2\left(1 - \frac{b^2}{r^2}\right) \equiv g(r). \tag{B.3}$$

The classical procedure is then to search for a minimum approach distance r_m. This is done demanding $\dot{r}^2 = g(r_\mathrm{m}) = 0$ in the preceding equation. There may be no root for r_m. Let us for example consider the dipole induced potential $U(r) = V(r)/\mu$ where $V(r)$ is taken from Eq. (4). The resulting equation for r_m is quadratic, and it is a matter of straightforward algebra to show that a root exists only if $b \geq b_0$, where b_0 is given by Eq. (6). In the opposite case, the distance is expected to decrease to zero. However, with a more realistic potential presenting a repulsive core at small distance, there will *always* be a root for r_m: at infinity, Eq. (B.3) gives $g(r) = v^2 > 0$ while at small distance, as $U(r) > 0$, obviously Eq. (B.3) gives $g(r) < 0$.

r_m corresponds to a polar angle θ_m, and it is easy to see that the defection angle χ is related to θ_m by

$$\chi = 2\theta_\mathrm{m} + \pi. \tag{B.4}$$

θ_m itself can be deduced from the fact that at infinity before the encounter, we have $\theta = -\pi$:

$$\theta_\mathrm{m} + \pi = \int_{r_\mathrm{m}}^{+\infty} \left|\frac{\mathrm{d}\theta}{\mathrm{d}r}\right| \mathrm{d}r = \int_{r_\mathrm{m}}^{+\infty} \frac{\dot{\theta}}{|\dot{r}|}\,\mathrm{d}r = \int_{r_\mathrm{m}}^{+\infty} \frac{bv}{r^2}\frac{\mathrm{d}r}{\sqrt{g(r)}}\,, \tag{B.5}$$

where $g(r)$ is defined in Eq. (B.3). Setting $y = r_\mathrm{m}/r$, this expression may be rewritten as

$$\theta_\mathrm{m} + \pi = \frac{b}{r_\mathrm{m}}\int_0^1 \frac{\mathrm{d}y}{\sqrt{1 - y^2 + \frac{2}{v^2}\left[y^2U(r_\mathrm{m}) - U(r_\mathrm{m}/y)\right]}}, \tag{B.6}$$

from which we derive straightforwardly

$$\chi(b, v) = \frac{2b}{r_\mathrm{m}}\int_0^1 \frac{1}{\sqrt{1 - y^2}}\frac{\mathrm{d}y}{\sqrt{1 + \epsilon(b, v, y)}} - \pi, \tag{B.7}$$

where

$$\epsilon(b, v, y) = \frac{2}{v^2}\frac{y^2U(r_\mathrm{m}) - U(r_\mathrm{m}/y)}{1 - y^2}. \tag{B.8}$$

This last expression is of practical interest to numerically compute χ for any potential: $\epsilon(b, v, y)$ has a finite limit towards $y \to 1$, so that the presence of the kernel $1/\sqrt{1 - y^2}$ allows a rapid computation using a Gauss-Chebychev quadrature technique.

Once χ is known, the impulsion change to the ion during the encounter reads

$$\delta\boldsymbol{p} = \mu v \begin{vmatrix} \cos\chi - 1 \\ \sin\chi\cos\phi \\ \sin\chi\sin\phi, \end{vmatrix} \tag{B.9}$$

once written in a Cartesian (x, y, z) referential frame with the x-axis parallel to the initial motion of the ion, and where ϕ is an azimuthal angle characterising the plane of the encounter. Of course over many encounters ϕ is a random angle, so that the y and z components of $\delta\boldsymbol{p}$ vanish. On average then, we have

$$\delta\boldsymbol{p} = \mu(\cos\chi - 1)\,\boldsymbol{v} = -2\mu\sin^2\left(\frac{\chi}{2}\right)\boldsymbol{v}. \tag{B.10}$$

Then follows a classical cross-section calculation. The number of encounters occurring within the time-span δt at (b, ϕ) within $\mathrm{d}b$ and $\mathrm{d}\phi$ is $nv\,\delta t\,b\,\mathrm{d}b\,\mathrm{d}\theta$. Multiplying then $\delta\boldsymbol{p}$ by this number of encounters and integrating over θ and b, we derive the drag force as:

$$\begin{aligned}\boldsymbol{f} &= \frac{1}{\delta t}\iint \delta\boldsymbol{p}(b, v)\,nv\,\delta t\,b\,\mathrm{d}b\,\mathrm{d}\theta \\ &= -4\pi n\mu v\left[\int_0^{+\infty} b\,\sin^2\left(\frac{\chi(b, v)}{2}\right)\mathrm{d}b\right]\boldsymbol{v}.\end{aligned} \tag{B.11}$$

If the collision is not elastic, the modulus of the relative velocity v' after the encounter differs from the initial one v. We have $v' = ev$. The impulsion change to the ion during the encounter reads now

$$\delta\boldsymbol{p} = \mu \begin{vmatrix} v\cos\chi - ev \\ v\sin\chi\cos\phi \\ v\sin\chi\sin\phi. \end{vmatrix} \tag{B.12}$$

As in the elastic case, there is no average change perpendicular to the motion. In the direction of the motion, we derive

$$\delta\boldsymbol{p} = \left(-2\mu e\sin^2\left(\frac{\chi}{2}\right) + (e - 1)\mu\right)\boldsymbol{v}. \tag{B.13}$$

Integrating as above over b and θ we derive the drag force as

$$\boldsymbol{f} = -2\pi n\mu v\left[\int_0^{+\infty}\left(2e\sin^2\left(\frac{\chi(b, v)}{2}\right) + 1 - e\right)b\,\mathrm{d}b\right]\boldsymbol{v}. \tag{B.14}$$